ADVANCED ENGINEERING MATERIALS
www.aem-journal.com

Transformation Pathway upon Heating of Ti–Fe Alloys Deformed by High-Pressure Torsion

Mario J. Kriegel, Askar Kilmametov, Martin Rudolph, Boris B. Straumal, Alena S. Gornakova, Hartmut Stöcker, Yulia Ivanisenko, Olga Fabrichnaya, Horst Hahn, and David Rafaja*

The current work presents the results of a study of the thermal stability of metastable ω-Ti(Fe) produced by a high-pressure torsion process and describes the phase transformations of ω-Ti(Fe) upon heating. The titanium alloys under study contain between 1 and 7 wt% of iron, the phase transitions are investigated using a combination of in situ high-temperature X-ray diffraction and differential scanning calorimetry. The high-temperature X-ray diffraction reveals the phase sequence $\omega \rightarrow \alpha' \rightarrow \alpha + \beta \rightarrow \beta$ upon heating. The differential scanning calorimetry shows that the first phase transformation is exothermal and that the temperature of this phase transition is independent of the iron concentration within the composition range under study. Subsequent phase transitions are endothermal and the respective transition temperatures depend on the iron concentration. The differences between the phase stabilities conclude from the phase diagram and the phase stabilities observe experimentally are explained by the partial coherence of the α/α′-Ti and β-Ti grains.

1. Introduction

Titanium alloys exhibit high strength, low density, and excellent corrosion resistance, thereby making them attractive for a variety of applications.[1] Nevertheless, new approaches are still required to further improve the properties of these materials. In particular, the mechanical properties of Ti-based alloys can be further improved via severe plastic deformation (SPD).[2,3] The SPD methods enable the production of bulk, nanostructured materials with unique mechanical properties, but they may also induce undesirable phase transformations and other concomitant microstructure changes.[4–8] For titanium and titanium alloys, the initiation of phase transformations by high-pressure torsion (HPT), which is one of the SPD techniques, was already reported in literature.[9–14] However, thermal stability studies of the of the HPT-induced phases in Ti-based alloys are scarce.[15,16]

Titanium exhibits three allotropic modifications: the low-temperature α-Ti phase with the space group (SG) $P6_3/mmc$, the high-temperature β-Ti phase (SG: $Im\bar{3}m$) and the high-pressure ω-Ti phase (SG: $P6/mmm$). In the Ti–Fe system, several metastable phases were reported, which form as a result of quenching from the bcc-type β solid solution.[17] For low Fe contents ($\leq$5 wt% Fe), the hexagonal close packed α'-martensite (SG: $P6_3/mmc$) can be obtained after quenching,[17–20] whereas in a limited compositional range between 3 and 5 wt% Fe, the formation of athermal ω-Ti(Fe) (SG: $P6/mmm$) was reported.[20–25] At higher Fe contents, the β phase remains as a metastable phase in the samples after quenching.

In Ti–Fe alloys subjected to HPT, the compositions at which the high-pressure ω phase exists are usually extended. Recently, a stabilization of the ω phase in these alloys containing between 0.5 and 4 wt% Fe was reported to be a product of the phase transitions $\alpha' \rightarrow \omega$ and $\beta \rightarrow \omega$ driven by HPT.[10,11] In a Ti–Fe alloy with an iron content of 1 wt%, the ω phase was found to be present with the hexagonal α/α' phase. On the other hand, the microstructure of the Ti–Fe alloys after the HPT process containing 4 wt% Fe consisted almost solely the ω phase.[10,11,13]

Still, very little is known about the high-temperature stability of metastable phases in the Ti–Fe system, and there is almost no information about the stability of ω-Ti(Fe). For example, only two alloy compositions (1 and 10 wt% Fe) were investigated by means of thermal analysis.[13] Furthermore, the transformation pathway upon heating starting from a highly deformed SPD state was not described yet. Therefore, in the present contribution, the

Dr. M. J. Kriegel, M. Rudolph, Dr. O. Fabrichnaya, Prof. Dr. D. Rafaja
TU Bergakademie Freiberg, Institute of Materials Science, 09599 Freiberg, Germany
E-mail: Mario.Kriegel@iww.tu-freiberg.de

Dr. A. Kilmametov, Prof. Dr. B. B. Straumal, Prof. Dr. Yu. Ivanisenko, Prof. Dr. H. Hahn
Karlsruhe Institute of Technology (KIT), Institute of Nanotechnology, 76344 Eggenstein-Leopoldshafen, Germany

Prof. Dr. B. B. Straumal, Dr. A. S. Gornakova
Institute of Solid State Physics, Russian Academy of Sciences, 142432 Chernogolovka, Russia

Prof. Dr. B. B. Straumal
Laboratory of Hybrid Nanomaterials, National University of Science and Technology «MISIS», 119049 Moscow, Russia

Dr. H. Stöcker
TU Bergakademie Freiberg, Institute of Experimental Physics, 09599 Freiberg, Germany

The ORCID identification number(s) for the author(s) of this article can be found under https://doi.org/10.1002/adem.201700933.

DOI: 10.1002/adem.201700933

microstructure changes of Ti–Fe alloys (ranging from 1 to 7 wt% Fe), which were observed during in situ high-temperature XRD (HTXRD) experiments, are correlated with the thermal behavior concluded from the thermal analysis measurements.

2. Experimental Section

Ti–Fe alloys containing 1, 2.2, 4, and 7 wt% Fe were prepared by inductive melting of high purity materials (99.9% Ti and 99.97% Fe). The melt was cast into a water-cooled copper crucible having a diameter of 10 mm. The as-cast cylinders were cut into disks with a thickness of approx. 1 mm. The disks were polished, etched, and placed in silica ampoules. The ampoules where then evacuated to a residual pressure of 4×10^{-4} Pa, sealed and annealed. The annealing temperatures were chosen to lie above the T_0-line (cf. **Figure 1**), that is, 950 °C for Ti–1Fe, 800 °C for Ti–2.2Fe and Fe–4Fe, and 580 °C for Ti–7Fe. The annealing times were 100, 120, 237, and 840 h, respectively. After annealing, the samples were quenched from the heat treatment temperature by immersing directly into water at room temperature. Following this, the samples were deformed by high-pressure torsion (HPT) in a Bridgman anvil-type unit. The HPT treatment was carried out at room temperature in a custom-built computer-controlled HPT device (W. Klement GmbH, Austria). The applied pressure was 7 GPa, the deformation speed was 1 rotation per minute and the overall number of rotations was 5.

The initial microstructures of the alloys Ti–1Fe, Ti–2Fe, and Ti–4Fe (before HPT deformation) were investigated by means of optical and scanning electron microscopy (OM and SEM, respectively). For these investigations, the samples were electropolished using a LectroPol-5 polishing device and the commercial electrolyte A-3 (both from Struers, Denmark). The SEM micrographs were performed using back-scattered electrons (SEM/BSE) with a FEG-SEM LEO 1530 GEMINI (Zeiss, Germany) operating at 20 kV.

High-temperature XRD measurements were carried out in symmetrical diffraction geometry on a θ/θ-diffractometer (Bruker D8 Discover, Germany) that was equipped with a Goebel mirror, a high-temperature chamber (Anton Paar DHS 1100, Austria) and a one-dimensional detector (Bruker LynxEye, Germany). Cu-$K\alpha$ radiation ($\lambda = 1.5418$ Å) was used, and during the in situ HTXRD measurements, the samples were placed on an AlN heating plate inside the high-temperature chamber, which was evacuated to a pressure of approx. 2×10^{-3} Pa. All HTXRD measurements were performed with a constant heating rate of 2 K min^{-1}. The diffraction patterns were collected in the 2θ range between 32 and 42° with a step size of 0.04° and with a measuring time of 2 s per step.

Thermal analysis measurements were performed to determine the transition temperatures of the phase transformations from the highly deformed metastable state after HPT toward the equilibrium state. For these measurements, a heat-flux differential scanning calorimeter (DSC, Netzsch Pegasus 404C, Germany) was employed. The samples were placed into Pt crucibles with very thin Al_2O_3 inlays to avoid contact between the metallic samples and the Pt crucible. Before each measurement, the system was evacuated and re-filled with high purity Ar (99.999% + Varian cleaning system) several times in order to remove remaining oxygen. The DSC measurements were done twice between 35 and 1100 °C using heating/cooling rates of 10 K min^{-1}. The device was calibrated to the melting temperatures of pure elements (Ag, Au, Cu, and Sn).

3. Results and Discussion

The Ti-rich part of the Ti–Fe phase diagram including the T_0-line, as shown in Figure 1 was calculated using a thermodynamic database recommended by the Scientific Group Thermodata Europe (SGTE).[26] The calculated T_0-line is compared to the start

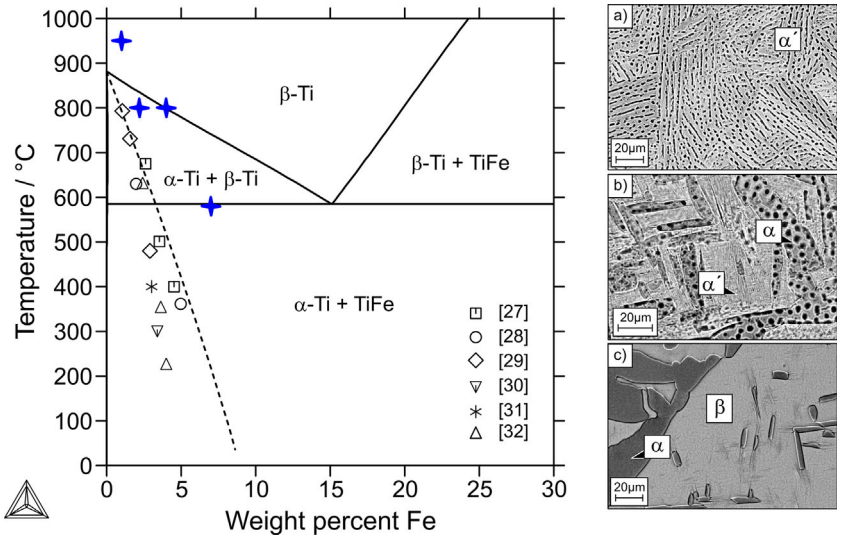

Figure 1. Phase diagram of the binary system Ti–Fe calculated using the database recommended from SGTE[26] including the T_0-line (dashed line) and the experimental $M_s(\alpha')$ points.[27–32] The chemical compositions and the annealing temperatures of the alloys are marked by blue stars. The SEM/BSE micrographs of a) Ti–1Fe, b) Ti–2.2Fe, and c) Ti–4Fe after water quenching are shown on the right hand side of this figure. Present phases are labelled by the symbols α, α', and β.

temperatures of the martensitic transformation determined experimentally.[27–32]

As the annealing temperatures were chosen above the T_0-line, sample Ti–1Fe was annealed within the single-phase β region, samples Ti–2.2Fe, and Ti-4Fe in the two-phase $\alpha + \beta$ region, and sample Ti–7Fe in the two-phase α + TiFe region according to the phase diagram (Figure 1). Different initial states of the samples were investigated in order to ensure the so-called "equi-final" state inside the samples. The amount of the torsion strain, which is necessary to initiate the phase transformations in the samples (e.g., $\alpha' \rightarrow \omega$; $\beta \rightarrow \omega$), strongly depends on their initial state. However, as the torsion strain reaches a certain saturation, the phase composition of all Ti–Fe alloys was the same, irrespectively, on the initial ones.[11]

Optical microscopy, scanning electron microscopy and X-ray diffraction revealed that the quenched sample Ti–1Fe contains α'-martensite, sample Ti–2.2Fe a mixture of α-Ti and α'-martensite, and sample Ti–4Fe a two-phase $\alpha + \beta$ microstructure with minor amounts of α' precipitates inside the β grains (cf. Figure 1). The α-Ti grains are coarse, globular, and embedded in the β matrix. The α'-martensite, which originates from the quenched β grains, possesses a plate-like morphology. On the other hand, sample Ti–7Fe contains a mixture of α-Ti and (disordered) β-Ti(Fe). The X-ray diffraction lines typical for the ordered TiFe phase are missing, thereby indicating very slow kinetics for the formation of this intermetallic phase.

During HPT, the quenched phases in samples Ti–1Fe, Ti–2.2Fe, and Ti–4Fe transformed into a $\omega + \alpha'$ two-phase mixture (see **Figure 2** at the bottom of each panel and **Figure 3** at low temperatures). However, the amount of α'-martensite decreased continuously with increasing Fe content, as can be seen in Figure 2 and 3. The HPT-processed sample Ti–4Fe contained almost only ω-Ti(Fe), as already reported in literature.[10,11] For Ti–7Fe, the β phase was found to coexist with ω after HPT. The coexistence of ω-Ti and β-Ti leads to a broad and asymmetrical intensity maximum below approx. 550 °C, which extends between 38.5 and 40°2θ (Figure 2).

In all HPT samples, two phase transitions were observed upon heating. Between 500 and 600 °C, ω-Ti transforms into the supersaturated hexagonal α'-martensite. The α'-Ti martensite possesses the same crystal structure as α-Ti, but can accommodate much more iron atoms than α-Ti, which exhibits only a negligible solubility for Fe.[23,33–35] As α'-Ti may contain higher amounts of Fe than α-Ti, the lattice parameters of α'-Ti are smaller than the lattice parameters of α-Ti.[10] Accordingly, the diffraction lines of α'-Ti are shifted to higher diffraction angles with respect to the diffraction lines of α-Ti. Since the transformation temperatures are below the eutectoid line $\beta \leftrightarrow \alpha$ + TiFe (cf. Figure 1), the β phase is not stable in this temperature range and the metastable high-pressure ω phase containing iron is forced to transform into α'-Ti. Some works showed that ω-Ti can transform perfectly to α'-Ti just by the presence of sufficient structural vacancies and that the vacancies can act as heterogeneous nucleation sites for α-Ti (or α'-Ti).[36,37]

Between 680 and 900 °C, the α' phase decomposes into the equilibrium phases α and β. In samples Ti–1Fe and Ti–2.2Fe, the diffraction lines from α-Ti are very broad and their positions are shifted toward lower diffraction angles. As mentioned above, the higher Fe content in α'-Ti as compared to α-Ti leads smaller lattice parameters. Furthermore, a higher concentration of Fe in α'-Ti reduces the c/a ratio.[10,17] This effect is responsible for the observed anisotropic line broadening. If the local concentration of Fe in α'/α-Ti varies, the line width increases with increasing diffraction index l, that is, from the diffraction line 100_α over 101_α to 002_α, not with the increasing magnitude of the diffraction vector, as it would be the case for a constant c/a ratio.

The "low-temperature" phase α-Ti is still present at very high temperatures above 950 °C in the samples. These temperatures are much higher than those corresponding to the phase diagram in Figure 1. This finding indicates slow kinetics of the phase transformation α-Ti $\rightarrow \beta$-Ti. A phenomenon possibly reducing the diffusion kinetics is the high concentration of microstructure defects produced during the HPT process. Still, it can be seen that the diffraction lines become sharper and more distinct upon heating. This indicates a reduction of the density of microstructure defects through their diffusion to the grain boundaries and annihilation, and via grain growth. Nevertheless, the kinetics of the phase transitions is very slow, which is demonstrated by the presence of α-Ti up to 1100 °C and by the fact that very long heat treatment durations are needed to reach the equilibrium state (see initial state of Ti–7Fe; above).

At 1100 °C, all investigated alloys should already have transformed to β-Ti. However, the diffraction line 100_α is clearly visible especially in samples Ti–4Fe and Ti–7Fe. The presence of the 100_α diffraction line up to very high temperatures can be explained by the presence of semi-coherent interfaces between α-Ti and β-Ti with the orientation relationship $(001)_\alpha \parallel (110)_\beta$ and $[110]_\alpha \parallel [\bar{1}11]_\beta$[38,39] and by the similarity of the atomic ordering within the almost parallel lattice planes $(100)_\alpha$ and $(1\bar{1}0)_\beta$ in this orientation relationship (cf. **Figure 4**). The interatomic distances within the lattice plane $(100)_\alpha$ are equal to $a_{\alpha\text{-Ti}}$ (2.951 Å) and $c_{\alpha\text{-Ti}}$ (4.679 Å); the interatomic distances within the lattice plane $(1\bar{1}0)_\beta$ are $a_{\beta\text{-Ti}}$ (3.311 Å) and $\sqrt{2} \times a_{\beta\text{-Ti}}$ (4.683 Å). This corresponds to lattice misfits of 11.5 and 0.1% in the respective directions (Figure 3). Within other lattice planes, the lattice misfit between α-Ti and β-Ti is much larger, leading to larger atomic disorder. Therefore, the most appreciable diffraction signal is produced by the lattice plane $(100)_\alpha$ and by the almost parallel lattice plane $(1\bar{1}0)_\beta$, which can be treated as habitus planes defining the α-Ti/β-Ti interface. Consequently, the semi-coherence of lattice planes $(100)_\alpha$ and $(1\bar{1}0)_\beta$ makes phase differentiation difficult. Therefore, intermediate states cannot be described as a simple phase mixture of α-Ti and β-Ti and are denoted as α/β within this article.

In the temperature range between 700 °C and approx. 950 °C, the α' phase seems to coexist with this α/β equilibrium phase mixture (see Figure 2). This phase coexistence can be explained by the fact that 1) the deformation state of HPT samples strongly depends on the distance from the center of the disc[3,40–42] and that 2) the α' phase regions located closer to the disc center will transform to the equilibrium phase assemblage (α/β) at lower temperatures than the strongly deformed areas close to the rim of the disc. Thus, the apparent coexistence of α'-Ti with the α/β-Ti is a consequence of the integrative character of the X-ray measurement.

In order to separate the overlapping diffraction lines in the in situ high-temperature XRD patterns and to (semi)quantify the phase transformation process, individual diffraction lines were fit by symmetrical Pearson VII functions[43] and their integral intensities employed as a measure of the phase contents (Figure 3).

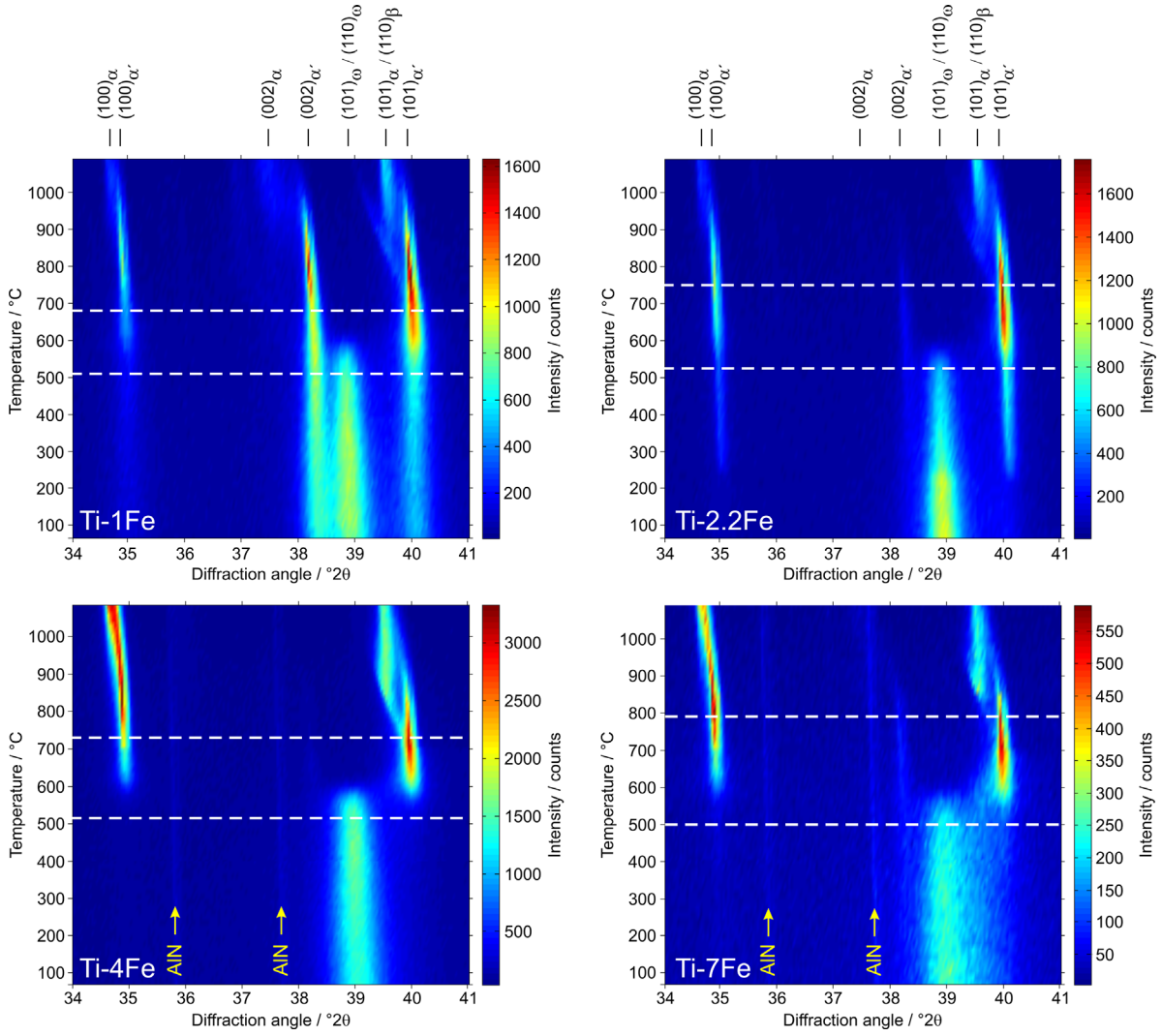

Figure 2. Low-angle parts of the XRD patterns measured in situ between room temperature and 1100 °C with a heating rate of 2 K min^{-1} for samples Ti–1Fe, Ti–2.2Fe, Ti–4Fe, and Ti–7Fe. The dashed lines indicate the starting temperatures of the phase transformations upon heating (see **Figure 3** for more details). Positions of diffraction lines stemming from individual titanium phases (α, α', ω, and β) are indicated at the top of the figure, positions of diffraction lines from the AlN heater are marked by yellow arrows.

The integrated intensities of the diffraction lines 100, 002, and 101 of α-Ti and α'-Ti were summed for each phase to improve the statistical reliability of the data and to reduce texture artefacts.

As already mentioned above, sample Ti–1Fe contains a significant amount of α'-Ti after the HPT treatment. The quantitative phase analysis using Rietveld refinement[44] revealed (66 ± 5) wt% of ω-Ti and (34 ± 4) wt% of α'-Ti. The transformation of ω-Ti to α'-Ti is significantly accelerated at 510 °C. At 625 °C, the sample consists mainly of α'-Ti. With further temperature increase, α'-Ti is not stable anymore and decomposes into the equilibrium phase mixture α/β. Above 900 °C, the α/β phase mixture becomes dominant, and at approx. 950 °C, the α' phase disappears almost completely. The sample Ti–2.2Fe contains (87 ± 2) wt% of ω-Ti and only (13 ± 1) wt% of α'-Ti after the HPT process. However, the transformation ω-Ti to α'-Ti starts earlier than in sample Ti–1Fe, already above 250 °C. Still, the remainder of ω-Ti are stable until approx. 600 °C. Between 600 and 900 °C, α'-Ti is the dominant phase until the α/β phase mixture becomes dominant above 900 °C.

Sample Ti–4Fe is almost single-phase after the HPT treatment. The intensities of the ω-Ti diffraction lines 101/110 stay constant up to 400 °C. The onset of the rapid phase transition from ω-Ti to α'-Ti is at 515 °C. Between 600 and 800 °C, α'-Ti is dominant, whereas the α/β mixture becomes dominant at higher temperatures. The diffraction line (100)α becomes very intense at high temperatures, thereby indicating the presence of atomic ordering along the lattice planes (100) of the original α'-Ti. As discussed above, the survival of α/α'-Ti is facilitated by the heteroepitaxy between α/α'-Ti and β-Ti having the mutual orientation relationship $(001)_\alpha \parallel (110)_\beta$ and $[110]_\alpha \parallel [\bar{1}11]_\beta$ and the habitus planes $(100)_\alpha$ and $(1\bar{1}0)_\beta$. Sample Ti-7Fe contains (91 ± 3) wt% of ω-Ti and (9 ± 1) wt% of β-Ti after the HPT treatment. The β-Ti(Fe) phase (disordered TiFe) is stabilized by the relatively high iron content, as shown in ref.[13] and by the slow transformation kinetics as

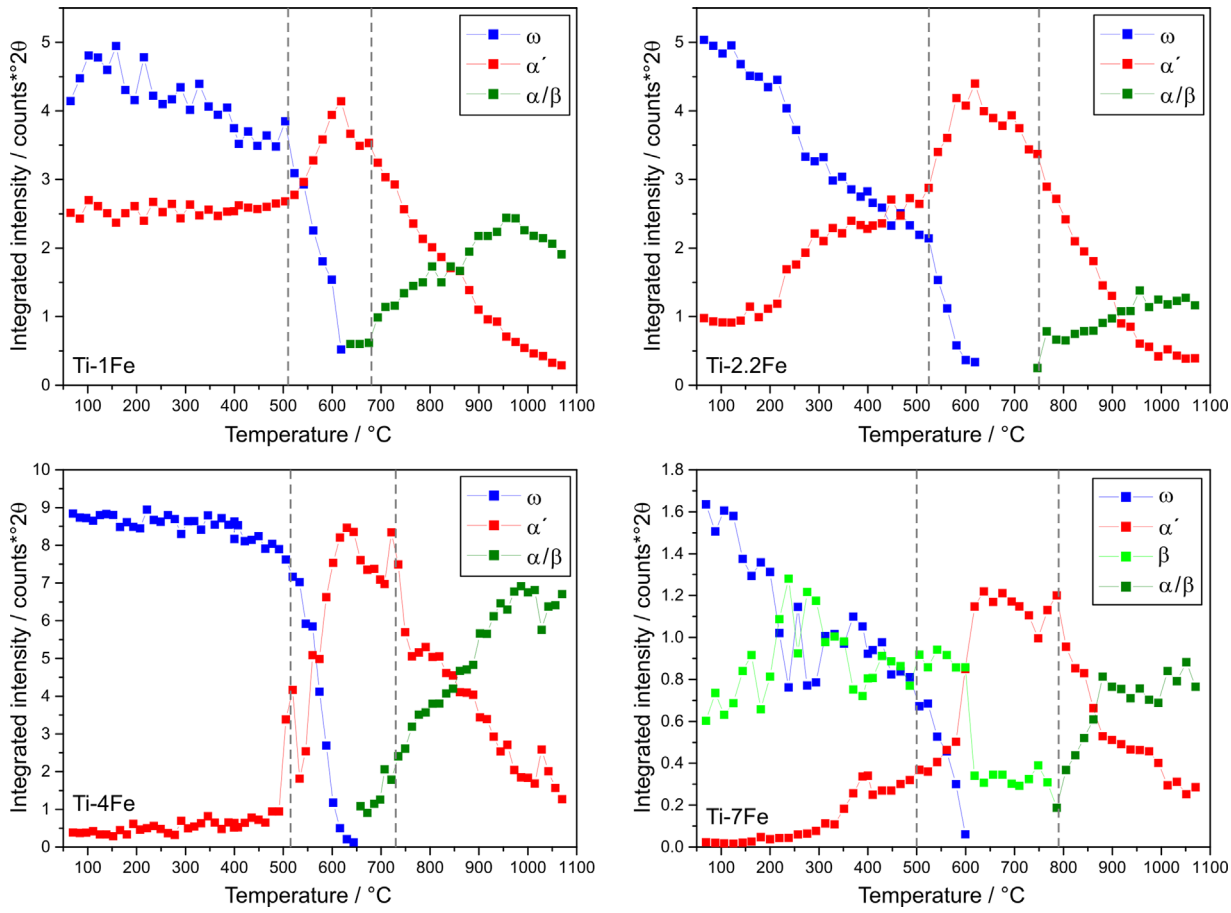

Figure 3. Temperature dependence of the integrated intensities of the diffraction lines of ω, α', α, and β that were calculated from single peak fits of the in situ X-ray measurements (2θ range: from 34° to 41°). The 100, 002, and 101 diffraction lines of α and α' were summed up. The dashed lines indicate the onsets of the phase transformations $\omega \rightarrow \alpha'$ and $\alpha' \rightarrow \alpha + \beta$.

discussed above. The amount of ω-Ti in Ti-7Fe decreases gradually with increasing temperature. A faster transformation of ω-Ti to α'-Ti occurs at temperatures above 400 °C. The α' phase stays dominant up to 850 °C. Nevertheless, above 800 °C it is gradually replaced by α/β. At 900 °C, α'-Ti practically disappears with the exception of the bits of the hexagonal (α'-Ti) structure, which is partially coherent with α/β.

The in situ HTXRD was complemented by differential scanning calorimetry measurements. The DSC curves (**Figure 5**) show small and broadened exothermic effects between 150 °C and 350 °C, which can be correlated with 1) a gradual transformation of ω-Ti to α'-Ti (in samples Ti–1Fe, Ti–2.2Fe, and Ti–7Fe) and 2) the defect annihilation and recrystallization processes (in all samples). The annihilation of microstructure defects and an increase in the

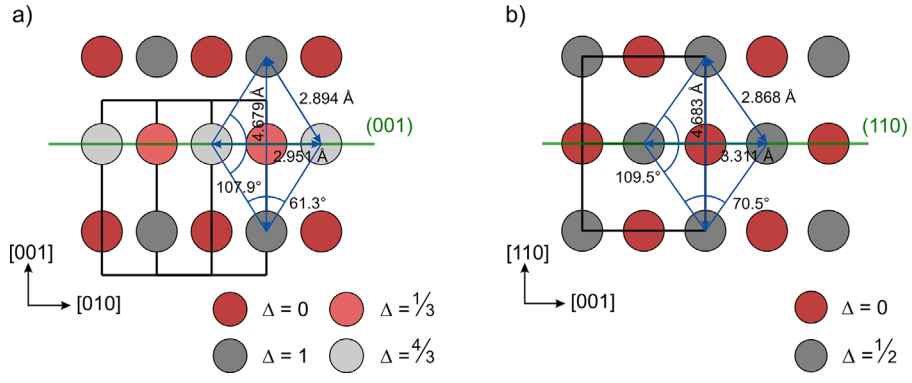

Figure 4. Projection of the a) α-Ti and b) β-Ti lattices to the almost parallel lattice planes $(100)_\alpha$ and $(1\bar{1}0)_\beta$, respectively. The displacement of the atoms from a reference plane (Δ) is given in multiples of a) $\sqrt{3}/2\ a_0$ and b) $\sqrt{2}\ a_0$, where a_0 is the lattice parameter of the respective crystal structure.

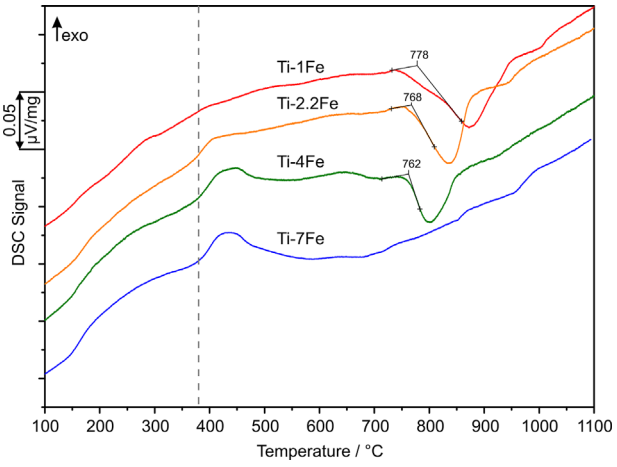

Figure 5. DSC heating curves of the individual samples after HPT using heating rates of 10 K min^{-1}. The dashed line indicates the onset of the transition of ω to α' and the given onset temperatures mark the decomposition of α' to α/β.

crystallite size were also detected in the XRD measurements through the sharpening of the diffraction lines. The first strong exothermal maximum in the DSC curves was observed between 380 and 485 °C. In this temperature range, the residual ω-Ti transforms to α'-Ti. The intensity of this DSC peak depends strongly on the amount of α'-Ti present after the HPT process. In sample Ti–1Fe, this peak is hardly visible, because this sample contained a large amount of α'-Ti already in the initial state. A less intense DSC peak in this temperature range was also observed in sample Ti-2.2Fe, in which the phase transition ω-Ti $\rightarrow$ α'-Ti is gradual. The strongest exothermic effects were measured in samples Ti–4Fe and Ti–7Fe, which contained almost no α'-Ti after the HPT treatment.

The onset temperatures shown in Figure 5 for Ti–1Fe, Ti–2.2Fe, and Ti–4Fe are associated with pronounced endothermal DSC peaks. They correspond to the decomposition of α'-Ti into the equilibrium phase mixture α/β, and to the transformation of the low-temperature phase α-Ti to the high-temperature phase β-Ti. In accordance with the phase diagram (Figure 1), the endothermic peak shifts to lower temperatures when the iron concentration in the samples increases. In sample Ti–7Fe, this peak is almost missing, since this sample contains permanently β-Ti and because the kinetics of the α'-Ti decomposition at high iron concentrations is slow (Figure 2, 3).

The results of the DSC measurements complement nicely the findings of in situ HTXRD. The ω-Ti phase is a high-pressure phase, which is retained as a metastable phase after the HPT process and the pressure release.[13,45] Upon heating, the latent heat stored in ω-Ti is released, thus an exothermic effect is detected by DSC. For the decomposition of the supersaturated α'-Ti phase into the equilibrium phases α-Ti and β-Ti and for the transition $\alpha + \beta \rightarrow \beta$, heat has to be provided to the sample in order to initiate the phase transitions that are connected with the endothermic heat effect in the DSC curve. The partial coherence between α-Ti and β-Ti, which is facilitated by their possible heteroepitaxy, leads to the stabilization of intermediate states during the $\alpha + \beta \rightarrow \beta$ transition and to a smearing and shifting of the transition temperatures. Consequently, various endothermic effects were observed between 820 and 1020 °C.

It should be noted that some differences in the transition temperatures measured by DSC and in situ HTXRD were detected. In contrast to the DSC measurements, the temperature measurement during in situ HTXRD was not performed exactly at the sample position, as the thermocouple was located below the AlN plate, separating the sample from the heater. Therefore, the temperatures measured during the HTXRD experiments were higher than the temperatures at the sample position. In the DSC device, a temperature calibration was performed to ensure the reliability of the determined transition temperatures.

4. Conclusions

Thermal stability of ω-Ti(Fe) and other microstructure features produced by the high-pressure torsion in titanium alloys containing 1–7 wt% Fe was investigated and correlated with the deformation microstructures. At low Fe contents ($\leq$2.2 wt%), the severely deformed samples contained a mixture of α'-Ti and ω-Ti(Fe). Higher amounts of iron like in the sample with 7 wt% Fe stabilize β-Ti as a secondary phase to ω-Ti(Fe). The in situ high-temperature X-ray diffraction measurements revealed that the transformation pathway upon heating is $\omega \rightarrow \alpha' \rightarrow \alpha + \beta \rightarrow \beta$. Metastable ω-Ti(Fe) transforms to α'-Ti at 380 °C. The results of differential scanning calorimetry show that this phase transformation is exothermic and confirmed that the temperature of this exothermal phase reaction does not change with the iron concentration in the Ti–Fe alloys in the concentration range under study. The decomposition of the oversaturated α'-Ti to α-Ti and β-Ti is endothermic and the transformation temperature decreases with increasing Fe content in the sample.

Acknowledgements

The work was partially supported by German Research Foundation (grant numbers FA999/1-1, IV 98/5-1, HA 1344/32-1, RA 1050/20-1), Russian Foundation for Basic Research (grant numbers 16-53-12007, 16-03-00285), Ministry of Education and Science of the Russian Federation in the framework of the Program to Increase the Competitiveness of NUST "MISiS", and Karlsruhe Nano Micro Facility.

Conflict of Interest

The authors declare no conflict of interest.

Keywords

Fe-Ti, high-pressure torsion, in situ high-temperature XRD, kinetics, omega-Ti, thermodynamics, transformation pathway

Received: October 24, 2017
Revised: December 8, 2017
Published online:

[1] G. Lütjering, J. C. Williams, *Titanium*, Springer Berlin Heidelberg, Berlin, Heidelberg **2007**.
[2] R. Z. Valiev, R. K. Islamgaliev, I. V. Alexandrov, *Prog. Mater. Sci.* **2000**, *45*, 103.
[3] A. P. Zhilyaev, T. G. Langdon, *Prog. Mater. Sci.* **2008**, *53*, 893.

[4] S. Gatina, I. Semenova, J. Leuthold, R. Valiev, *Adv. Eng. Mater.* **2015**, *17*, 1742.
[5] Y. Ivanisenko, A. Kilmametov, H. Rösner, R. Z. Valiev, *Int. J. Mater. Res.* **2008**, *99*, 36.
[6] I. P. Semenova, A. V. Polyakov, V. V. Polyakova, Y. Huang, R. Z. Valiev, T. G. Langdon, *Adv. Eng. Mater.* **2016**, *18*, 2057.
[7] A. V. Sergueeva, V. V. Stolyarov, R. Z. Valiev, A. K. Mukherjee, *Scr. Mater.* **2001**, *45*, 747.
[8] R. Valiev, *Nat. Mater.* **2004**, *3*, 511.
[9] K. Edalati, T. Daio, M. Arita, S. Lee, Z. Horita, A. Togo, I. Tanaka, *Acta Mater.* **2014**, *68*, 207.
[10] A. Kilmametov, Y. Ivanisenko, B. Straumal, A. A. Mazilkin, A. S. Gornakova, M. J. Kriegel, O. B. Fabrichnaya, D. Rafaja, H. Hahn, *Scr. Mater.* **2017**, *136*, 46.
[11] A. R. Kilmametov, Y. Ivanisenko, A. A. Mazilkin, B. B. Straumal, A. S. Gornakova, O. B. Fabrichnaya, M. J. Kriegel, D. Rafaja, H. Hahn, *Acta Mater.* **2018**, *144*, 337.
[12] B. Straumal, A. Korneva, P. Zięba, *Arch. Civ. Mech. Eng.* **2014**, *14*, 242.
[13] B. B. Straumal, A. R. Kilmametov, Y. Ivanisenko, A. S. Gornakova, A. A. Mazilkin, M. J. Kriegel, O. B. Fabrichnaya, B. Baretzky, H. Hahn, *Adv. Eng. Mater.* **2015**, *17*, 1835.
[14] C. T. Wang, A. G. Fox, T. G. Langdon, *J. Mater. Sci.* **2014**, *49*, 6558.
[15] Y. Huang, S. Mortier, P. H. R. Pereira, P. Bazarnik, M. Lewandowska, T. G. Langdon, *IOP Conf. Ser. Mater. Sci. Eng.* **2017**, *194*, 012012.
[16] A. Panigrahi, M. Böhnisch, T. Waitz, M. Calin, W. Skrotzki, J. Eckert, M. Zehetbauer, "Thermal stability of HPT-induced omega phase in biocompatible Ti-16.1Nb alloys", presented at *PTM-2015 - Proceedings of the 7th International Conference on Solid-Solid Phase Transformations in Inorganic Materials (PTM)*. Whistler, BC, Canada **2015**, pp. 263–268.
[17] J. L. Murray, *Bull. Alloy Phase Diagrams* **1981**, *2*, 320.
[18] A. V. Dobromyslov, V. A. Elkin, *Scr. Mater.* **2001**, *44*, 905.
[19] I. Levi, D. Shechtman, *Metall. Trans. A* **1989**, *20*, 2841.
[20] M. M. Stupel, M. Ron, B. Z. Weiss, *J. Appl. Phys.* **1976**, *47*, 6.
[21] S. Banerjee, P. Mukhopadhyay, *Phase Transformations*, Vol. *12*, Elsevier Science, Oxford, UK **2007**.
[22] T. W. Heo, D. S. Shih, L. Q. Chen, *Metall. Mater. Trans. A* **2014**, *45*, 3438.
[23] J. Matyka, F. Faudot, J. Bigot, *Scr. Metall.* **1979**, *13*, 645.
[24] G. I. Nosova, N. B. D'yakonova, I. V. Lyasotskii, *Met. Sci. Heat Treat.* **2006**, *48*, 427.
[25] S. K. Sikka, Y. K. Vohra, R. Chidambaram, *Prog. Mater Sci.* **1982**, *27*, 245.
[26] P. Franke, D. Neuschütz, in *Thermodynamic Properties of Inorganic Materials. Binary Systems, Part 3: Binary Systems from Cs—K to Mg—Zr* Vol. 19, Springer Berlin/Heidelberg, Aachen **2005**.
[27] P. Duwez, *Trans. Am. Soc. Met.* **1953**, *45*, 935.
[28] Y. N. Gridnev, Y. N. Petrov, V. A. Rafalovskiy, V. I. Trefilov, *Vopr. Fiz. Met. Metalloved. Ukr. SSR Sb. Nauchn. Rabot* **1960**, *11*, 82.
[29] H. Kaneko, Y. C. Huang, *J. Jpn. Inst. Met.* **1963**, *27*, 393.
[30] V. N. Moiseev, *Metalloved. Term. Obrab. Met.* **1969**, *2*, 335.
[31] T. Sato, S. Hukai, Y. C. Huang, *J. Aust. Inst. Met.* **1960**, *5*, 149.
[32] T. Yamane, M. Ito, "M_s and β(s) temperature of Ti — Fe alloys", presented at *Titanium 80, Sci. and Tech., Proc. 4th Int. Conf. Ti*, Kyoto, Japan **1980**.
[33] A. Blaesius, U. Gonser, *J. Phys. Colloq.* **1976**, *37*, 397.
[34] N. G. Boriskina, K. P. Myasnikova, *Akad. nauk SSSR* **1962**, *7*, 61.
[35] E. Raub, C. J. Raub, E. Röschel, V. B. Compton, T. H. Geballe, B. T. Matthias, *J. Less Common Met.* **1967**, *12*, 36.
[36] S. H. Kim, S. J. Kang, M. H. Park, C. W. Yang, H. C. Lee, H. N. Han, M. Kim, *Acta Mater.* **2015**, *83*, 499.
[37] C. Lin, G. Yin, A. Zhang, Y. Zhao, Q. Li, *Scr. Mater.* **2016**, *117*, 28.
[38] W. G. Burgers, *Physica* **1934**, *1*, 561.
[39] C. McHargue, *Acta Cryst.* **1953**, *6*, 529.
[40] A. Vorhauer, R. Pippan, *Scr. Mater.* **2004**, *51*, 921.
[41] Z. Yang, U. Welzel, *Mater. Lett.* **2005**, *59*, 3406.
[42] A. P. Zhilyaev, G. V. Nurislamova, B. K. Kim, M. D. Baró, J. A. Szpunar, T. G. Langdon, *Acta Mater.* **2003**, *51*, 753.
[43] M. M. Hall, Jnr, V. G. Veeraraghavan, H. Rubin, P. G. Winchell, *J. Appl. Crystallogr.* **1977**, *10*, 66.
[44] J. Rodríguez-Carvajal, *Physica B* **1993**, *192*, 55.
[45] J. C. Jamieson, *Science* **1963**, *140*, 72.

